

# Voltage Parameter Identification of AC Overhead Transmission Lines by Using Measured Electric Field Data

Dongping Xiao, Qi Zheng, Yutong Xie, Qichao Ma, and Zhanlong Zhang

State Key Laboratory of Power Transmission Equipment & System Security and New Technology  
Chongqing University, Chongqing, 400044, China

xiaodongping@cqu.edu.cn, 20161113031t@cqu.edu.cn, 20151102059t@cqu.edu.cn, 20151113002t@cqu.edu.cn,  
zhangzl@cqu.edu.cn

**Abstract** — With the development of smart power grids, the demand for real-time voltage monitoring along overhead transmission lines (OTLs) has been growing. However, the existing voltage measurement of OTLs by using potential transformers involves formidable difficulties. This study proposes a non-contact measurement method in which the voltages on AC OTLs are inversely calculated on the basis of the measured data of the power frequency electric field under OTLs. To improve the accuracy and stability of the inverse calculation, an accurate mathematical model and modified inverse algorithms are investigated and then a set of feasible approaches are proposed. First, considering an overhead conductor's actual physical form and the meteorological conditions of its operating environment, a 3-D catenary model is built, and the mathematical relations between 3-D electric fields and the voltages on OTLs are identified. Second, the improved particle swarm algorithm is used to search the optimal measurement positions of the electric field to improve the ill-posedness of inverse problems. Third, the iterative Tikhonov regularization method, in which the number of iterations is considered as the variable, is adopted to further improve the ill-posedness of inverse problems and reduce the susceptibility of regular solutions to regularization parameter  $\alpha$ . Fourth, root mean square values and phase parameters of AC voltages are identified from the sinusoidal fitting curves obtained by the real-time inverse calculation. Results of the simulation and experiment examples show that inverse solutions of high precision can be obtained under the condition with relatively high errors of electric field measurement. Moreover, the advantages of the proposed inversion method, such as fast computing speed and good stability, are demonstrated.

**Index Terms** — 3-D model, AC overhead transmission lines, electric field, inversion, iterative Tikhonov regularization, parameter identification, position optimization, voltage.

## I. INTRODUCTION

Root mean square (RMS) values and voltage phase of AC overhead transmission lines (OTLs) reflect the operating status and health level of power grids. The conventional method of measuring voltages on OTLs is to use the potential transformers that are installed in substations. With the development of smart power grids, the demand for real-time voltage monitoring along OTLs has become increasingly apparent. However, installing a large number of potential transformers along operating OTLs is not feasible because of certain formidable difficulties, such as the requirement for power-off installation and the increasing probability of ferro-resonance and insulation fault [1-2]. Given such bottleneck, studying new voltage measurement methods is necessary.

Numerous studies on the electromagnetic environment of high-voltage OTLs reveal that the power-frequency electric field around OTLs is significantly correlated with the power-frequency voltages on OTLs [3-5]. On the basis of this correlation, we propose the idea of inversely calculating voltages by using the measured data of the electric field. This non-contact voltage measurement has prominent advantages in safety and operation flexibility. The main challenge in applying this method to engineering is the improvement of the accuracy and stabilization of the inverse calculation. Calculation accuracy is influenced by the precision of electric field measurement on site and the precision of the mathematical model and inversion algorithm. This study focuses on the latter.

In most studies, 2-D models that ignore the sag and span of OTLs and other factors have been used to assess the electric field around OTLs [4-6]. However, these 2-D models are too rough to solve the proposed inverse problem. Certain studies have built a 3-D simulation model but only with consideration of equally high suspension case and a limited length of OTLs [7-8]. In the present study, considering the actual meteorological and orographic environment and the physical form of

OTLs, the 3-D model of OTLs is built, and then the mathematical relations between the 3-D electric fields and voltages are proposed.

The calculation of voltages on AC OTLs based on measured electric field data is an electromagnetic inverse problem, which has serious ill-posedness. Many studies have been devoted to dealing with the ill-posed problem [9-13], in which Tikhonov regularization has been widely used. The error between the solution of Tikhonov regularization and the true value strongly depends on the value of regularization parameter  $\alpha$ , and minor differences in  $\alpha$  may lead to distinctly different inverse solutions. For the selection strategy of  $\alpha$ , priori estimate and posterior estimate are available [14-17]. Priors estimate requires some priori information of the true value, but obtaining it in practical engineering applications is difficult. By contrast, posterior estimate is based on measured data and error level. From posterior estimate, several specific methods have been developed, and they include the Morozov's discrepancy principle, generalized cross inspection criteria, and L-curve criterion. However, the process of  $\alpha$ -selection based on the methods mentioned above is tedious, and the reselection of  $\alpha$  is required when the measurement error level changes. After analyzing the causes of ill-posedness in the special inverse problem, this study proposes a series of approaches that search the optimal positions of electric field measuring points to reduce the condition number of the observation matrix. Then, iterative Tikhonov regularization is processed to obtain inverse solutions point by point in the time domain.

## II. MATHEMATICAL MODEL AND OPTIMIZATION METHOD

### A. 3-D model of OTLs' voltage and electric field

Given the self-heavy, wind and ice load on OTLs and other factors, an OTL suspended between two towers is in the shape of catenary. For universal situations, a suspended OTL of unequal height (Fig. 1) is considered. In Fig. 1, the coordinate origin is set at the ground projection of the left suspension point.

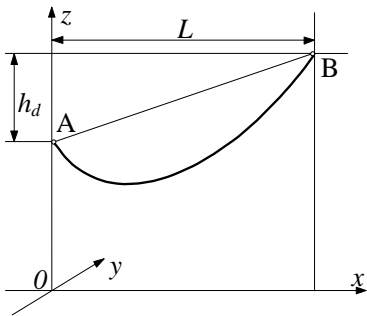


Fig. 1. Structural diagram of suspended OTL of unequal height.

The catenary can be described by Equation (1) [18]:

$$z(x) = \frac{h_d}{a \sinh(L/a)} \left[ a \sinh\left(\frac{x}{a}\right) \sinh\left(\frac{L-x}{a}\right) \right] - \sqrt{1 + \left(\frac{h_d}{a \sinh(L/a)}\right)^2}, \quad (1)$$

where  $a=2\sigma_0/\gamma$  is defined as the sag coefficient in which  $\sigma_0$  is the horizontal stress of the conductor and  $\gamma$  is the conductor load,  $h_d$  is the height difference between the two suspension points, and  $L$  is the line span.

When  $h_d = 0$ , OTLs are suspended at equal heights, and the corresponding catenary equation can be simplified to the following:

$$z(x) = -a \sinh(x/a) \sinh[(L-x)/a] \quad (0 \leq x \leq L). \quad (2)$$

Parameters  $\sigma_0$  and  $\gamma$  depend on the mechanical and physical characteristic of OTL, length of span, and weather conditions [19-20]. They can be calculated on the basis of given operating conditions. The introduction of these parameters helps improve the accuracy of the electric field calculation. Considering that phase conductors of the same type in the same span have a uniform catenary form is reasonable.

One phase of high-voltage OTLs usually contains a bundle of sub-conductors. When the radius of a circle, along which the bundled sub-conductors are arranged, is smaller than the distance between the conductors and observation point, such bundle can be equivalent to one conductor.

Power frequency electric field can be regarded as quasi-static electric field. The electric field generated by AC OTLs is usually calculated with the Charge Simulation Method [21-23], in which the effect of the conducting ground is equivalent to that of mirror image conductors. Suppose that the  $n^{\text{th}}$  phase conductor is  $l_n$  and that its mirror image is  $l'_n$ . Their equivalent charge densities are  $+\tau_n$  and  $-\tau_n$ . The potential at the spatial observation point  $C(x_m, y_m, z_m)$  is given by the following:

$$U_{nm} = \frac{1}{4\pi\epsilon_0} \left[ \int_{l_n} \left( \frac{1}{R_{nm}} - \frac{1}{R'_{nm}} \right) \tau_n dl_n \right], \quad (3)$$

where  $\epsilon_0$  is the dielectric constant of air and  $R_{nm}$  and  $R'_{nm}$  are the distances from the  $n^{\text{th}}$  phase conductor and its mirror image to the observation point  $C$ , respectively:

$$\mathbf{R}_{nm} = (x_m - x_n) \mathbf{e}_x + (y_m - y_n) \mathbf{e}_y + (z_m - z_n) \mathbf{e}_z,$$

$$\mathbf{R}'_{nm} = (x_m - x_n) \mathbf{e}_x + (y_m - y_n) \mathbf{e}_y + (z_m + z_n) \mathbf{e}_z,$$

$$R_{nm} = |\mathbf{R}_{nm}|, \quad R'_{nm} = |\mathbf{R}'_{nm}|.$$

The spatial structure for the calculation is shown in Fig. 2.

Equations (1) or (2) are substituted into (3) and the integral variable is converted into  $x_n$ . The discretization and numerical integration are carried out by using the Method of Moment. With the synthetical consideration of computational complexity and accuracy, the  $(2K+1)$

continuous spans of OTLs near point  $C$  are intercepted to calculate the potential.

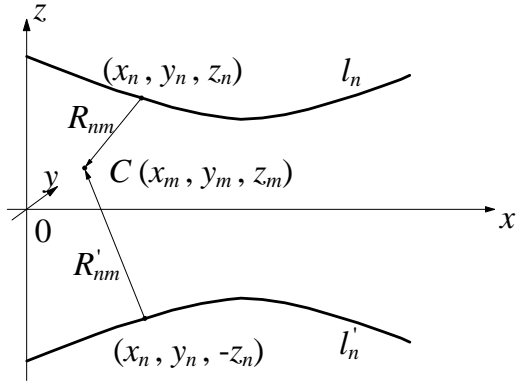


Fig. 2. Diagram of the spatial structure for calculation.

Point  $C$  is named as the match point if it is set on the surface of the phase conductor. The potential at point  $C$  is generated by the total  $N$  phases of OTLs. Then, the mathematical relationship between the known surface potential and the simulated charge density is expressed in matrix form as:

$$\mathbf{U} = \mathbf{P}\boldsymbol{\tau}, \quad (4)$$

where  $\mathbf{P}$  is an  $N$ -dimensional square matrix and the elements in  $\mathbf{P}$  can be calculated by numerical integration according to Equation (3).

Then, the 3-D electric field components at point  $C$  are calculated by the following:

$$\mathbf{E}_m(x, y, z) = \frac{1}{4\pi\epsilon_0} \sum_{n=1}^N \left[ \int_{l_n} \left( \frac{\mathbf{R}_{nm}}{R_{nm}^3} - \frac{\mathbf{R}'_{nm}}{R'_{nm}{}^3} \right) \tau_n dl_n \right] \quad (5)$$

$$= E_{mx} \mathbf{e}_x + E_{my} \mathbf{e}_y + E_{mz} \mathbf{e}_z.$$

By setting  $M$  measuring points, the matrix equation can be written as follows:

$$\mathbf{E} = \mathbf{G}\boldsymbol{\tau}. \quad (6)$$

According to Equations (4) and (6), the mathematical relationship between the surface potential of OTLs and the electric fields at the measuring points is given by the following:

$$\mathbf{E} = \mathbf{G}\mathbf{P}^{-1}\mathbf{U} = \mathbf{K}\mathbf{U}, \quad (7)$$

where  $\mathbf{K}$  is defined as the observation matrix.

Errors and noises inevitably exist in actual measurements. Only  $E^\delta$  ( $\|E - E^\delta\| < \delta$ ) can be obtained. If the positions of the measuring points are selected randomly, the condition number of matrix  $\mathbf{K}$  (i.e.,  $\text{cond}(\mathbf{K})$ ) may be large. Consequently, a small noise in  $\mathbf{E}$  may cause the inverse solution  $\mathbf{U}^\delta$  to severely deviate from the true value  $\mathbf{U}$ .

## B. Position optimization algorithm in 3-D space

Section II.A shows that the observation matrix  $\mathbf{K}$  is determined by the structure of OTLs and the positions of electric field measuring points. When the structure

of OTLs is fixed, reducing  $\text{cond}(\mathbf{K})$  by optimizing the positions of measuring points is convenient and feasible. It can reduce the susceptibility of inverse calculation to measurement noise [24].

In this study, the particle swarm optimization algorithm is adopted to search the optimal measuring positions. The fitness function of the algorithm is set as follows:

$$\text{FitFun} = \text{cond}(\mathbf{K}). \quad (8)$$

In the iteration process of searching the optimal solution, values of the fitness function of each particle are calculated and compared. Moreover, the historical optimal position of each individual particle  $\mathbf{X}_{Hbest}$ ,  $\mathbf{Y}_{Hbest}$ ,  $\mathbf{Z}_{Hbest}$  and the global historical optimal positions of the particle swarm  $\mathbf{X}_{Gbest}$ ,  $\mathbf{Y}_{Gbest}$ ,  $\mathbf{Z}_{Gbest}$  are dynamically updated, thereby guiding a convergence to the global optimal position. The velocities and positions of particles in the  $(i+1)^{\text{th}}$  generation of particle swarm on the  $x$ -axis are determined by the following [25]:

$$\mathbf{V}_x^{i+1} = \omega \mathbf{V}_x^i + c_1 r_{x1}^{i+1} (\mathbf{X}_{Hbest} - \mathbf{X}^i) + c_2 r_{x2}^{i+1} (\mathbf{X}_{Gbest} - \mathbf{X}^i), \quad (9a)$$

$$\mathbf{X}^{i+1} = \mathbf{X}^i + \mathbf{V}_x^{i+1}, \quad (9b)$$

where  $\omega$  is the inertia weight,  $c_1$  and  $c_2$  are two learning factors, and  $r_{x1}^{i+1}$  and  $r_{x2}^{i+1}$  are two random numbers with values ranging from 0 to 1, respectively.

The iteration processes of particle swarm on the  $y$ - and  $z$ -axis are similar to Equations (9a) and (9b).

The iterative process stops when it reaches the predetermined maximum iteration number or the predetermined fitness function threshold. Consequently, the global optimal fitness function value  $G_{best}$  and the corresponding optimal position  $\mathbf{X}_{Gbest}$ ,  $\mathbf{Y}_{Gbest}$ ,  $\mathbf{Z}_{Gbest}$  are the outputs.

## C. Iterative Tikhonov regularization method

The conventional Tikhonov regularization method turns the inverse calculation problem into a minimization problem [26]:

$$\begin{cases} \min J_\alpha(\mathbf{U}) \\ J_\alpha(\mathbf{U}) = \|\mathbf{K}\mathbf{U} - \mathbf{E}^\delta\|^2 + \alpha \|\mathbf{U}\|^2 \end{cases}, \quad (10)$$

where  $\alpha$  is the regularization parameter.

The approximate regularization solution can be obtained using the following expression:

$$\mathbf{U}_\alpha^\delta = (\alpha \mathbf{I} + \mathbf{K}^* \mathbf{K})^{-1} \mathbf{K}^* \mathbf{E}^\delta. \quad (11)$$

An iterative Tikhonov regularization method is proposed to achieve a high convergence order [27],

$$\begin{cases} \mathbf{U}_\alpha^{0,\delta} = 0 \\ \mathbf{U}_\alpha^{i,\delta} = \alpha (\alpha \mathbf{I} + \mathbf{K}^* \mathbf{K})^{-1} \mathbf{U}_\alpha^{i-1,\delta} + (\alpha \mathbf{I} + \mathbf{K}^* \mathbf{K})^{-1} \mathbf{K}^* \mathbf{E}^\delta \quad i=1,2,\dots \end{cases}, \quad (12)$$

where  $i$  is the iterative order number. When  $i=1$ , the conventional Tikhonov regularization is similar to

Equation (11).

The iterative Tikhonov regularization method can be implemented in two ways. One way is to select a fixed  $i$  ( $i \geq 1$ ), and perform the iterative calculation to achieve the optimization of  $\alpha(\delta)$ . Several studies have adopted this approach and developed certain selection criteria of  $\alpha(\delta)$ . However, the selection procedure of  $\alpha(\delta)$  is cumbersome, and  $\alpha(\delta)$  greatly influences inverse solutions. Once a slight change occurs in the analytical conditions,  $\alpha(\delta)$  must be reselected. Another way is to select a fixed  $\alpha$  ( $\alpha \geq 0$ ) that is determined by priori estimation and then perform the iterative calculation with the uncertain parameter  $i$ . The regularization solution can be obtained conveniently and quickly by reasonably setting the iterative termination conditions. Thus, the second approach is adopted.

The theorem in [27] is used to select  $\alpha$  and set the iterative termination conditions. Suppose that  $i(\delta)$  is the smallest integer that meets the iterative termination condition,

$$\| \mathbf{K} \mathbf{U}_\alpha^{i,\delta} - \mathbf{E}^\delta \| \leq \tau \delta \quad (\tau > 1). \quad (13)$$

A constant  $\alpha_0$  exists to make  $i \geq r + 1/2$  when  $\alpha \geq \alpha_0$ :

$$\alpha_0 = \frac{(2r+1) \| \mathbf{K} \|^2}{1 - \frac{(r+1)^2 \delta^2}{\| \mathbf{E} \|^2}} - \| \mathbf{K} \|^2. \quad (14)$$

#### D. Characteristic parameter determination of sinusoidal voltage

The characteristic parameters of the power frequency voltage are the RMS and phase. One approach is to use the phasors of electric field components to inversely calculate the phasors of voltages. This calculation process is simple, but the accuracy is not up to expectation. Another procedure is proposed in this study. The multi-point synchronous real-time electric field measurement is carried out by our self-made device. Then, the voltage value can be calculated point by point in the time domain according to the mathematical models and the optimization method described above. The characteristic parameters of sinusoidal voltages can be determined by the sinusoidal function fitting. This method has good anti-interference ability and self-tuning function, and thus, it can improve the calculation accuracy.

### III. NUMERICAL EXAMPLE AND ANALYSIS

#### A. Structure of OTLs and analysis condition

The selected simulation example involves 220 kV single-circuit OTLs. The phase conductor is 2×LGJ-400/35, and the length of the span is 300 m. Two suspension cases are shown in Figs. 3 (a) and 3 (b). Figure 3 (c) shows the layout of the phase conductors on each tower in Case I and on the left-side tower in Case II. Figure 3 (d) shows the layout of the phase conductors

on the right-side tower in Case II.

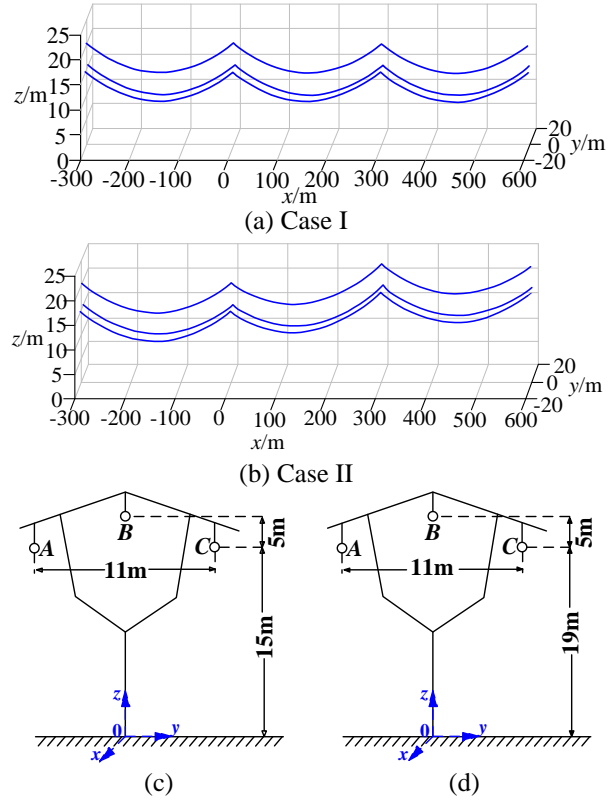


Fig. 3. Structure diagram of transmission line conductors.

Other analysis conditions are set as follows.

1) Three-phase symmetrical voltages of OTLs are:

$$\dot{\mathbf{U}} = \begin{bmatrix} \dot{U}_A \\ \dot{U}_B \\ \dot{U}_C \end{bmatrix} = \begin{bmatrix} 127.02 \angle 0^\circ \\ 127.02 \angle -120^\circ \\ 127.02 \angle 120^\circ \end{bmatrix} \text{ kV}.$$

2) Given the mathematical principle for solving matrix equations as well as the accessibility of the real-time and synchronous measurement of electric fields, three measuring points, which meet the minimum number of measuring points for calculating three-phase voltages, are set near the ground. In view of the structural symmetry of the three-phase OTLs, the three measuring points are symmetrically arranged relative to the y-axis on a cross section.

3) For the meteorological conditions, breezeless, ice-free, and average outdoor temperature conditions are assumed. Accurate values of the electric field can be calculated according to Equations (1)-(5), and the measured electric field data are simulated by adding the random white noise with the noise level of  $\sigma$ .

#### B. Position optimization of measuring points

For Case I, the space range of the position

optimization is set as  $0 \leq x \leq 150\text{m}$ ,  $-15\text{m} \leq y \leq 15\text{m}$ , and  $1\text{m} \leq z \leq 3\text{m}$ . The results of several optimizations are  $\text{cond}(\mathbf{K}) = G_{\text{best}} = 14.87$ , thus, the corresponding optimal measuring positions are (150 -7.5 3), (150 0 3), and (150 7.5 3).

Moreover, two sets of measuring points (10 -5 1), (10 0 1), (10 5 1) and (100 -10 2), (100 0 2), (100 10 2) are randomly selected, and the corresponding  $\text{cond}(\mathbf{K})$  is calculated.

Under the condition of 10% measurement error, the directly inverse calculation is performed to obtain the corresponding inverse solution  $\mathbf{U}^\delta$  at three sets of measuring points. The results of the inverse calculation are different because of the addition of random noise. The means and variances of 10 calculations are determined statistically, as shown in Table 1.

Table 1 shows that different positions of the measuring points lead to different  $\text{cond}(\mathbf{K})$  and  $\mathbf{U}^\delta$ . The greater the  $\text{cond}(\mathbf{K})$  is, the more  $\mathbf{U}^\delta$  deviates from the accurate  $\mathbf{U}$ . The greater the variance is, the worse the calculation stability appears. Thus, the position optimization of measuring points presents a significant improvement in the ill-posedness of inverse problems.

For Case II, the optimal measuring positions to be found are (120 -6.5 2.9), (120 0 3), (120 6.5 2.9), and the corresponding  $\text{cond}(\mathbf{K})$  is 29.74. The inverse solution  $\mathbf{U}^\delta$  obtained by the directly inverse calculation is as follows:

$$\dot{\mathbf{U}}^\delta = \begin{bmatrix} 136.91 \angle 1.57^\circ \\ 153.54 \angle -123.78^\circ \\ 135.13 \angle 117.68^\circ \end{bmatrix} \text{ kV}.$$

Compared with other randomly selected measuring points, the optimal measuring positions determines the minimum  $\text{cond}(\mathbf{K})$ . Moreover, the accuracy and stability of the inverse calculation are significantly improved. This outcome is similar to the conclusion in Case I.

Although the position optimization of measuring points improves the performance of the directly inverse calculation, the accuracy of inverse solutions requires further improvement. Thus, the iterative regularization method is required.

### C. Iterative Tikhonov regularization in time-domain

Suppose that the electric field data measured in real time with a noise level of 10% are obtained at the three optimal measuring points in Case I. The directly inverse calculation and the traditional Tikhonov regularization calculation with  $\alpha=10^{-6}$  and  $\alpha=10^{-5}$ , respectively, are performed. Figure 4 shows the comparison among

the accurate three-phase voltages and the three inverse solutions in a sinusoidal period. Figure 4 reveals that a certain error exists between the directly inverse solutions and accurate values. The accuracy of inverse solutions is improved when the single Tikhonov regularization calculation with  $\alpha=10^{-6}$  is carried out. However, the accuracy is significantly decreased when  $\alpha=10^{-5}$ . This result suggests that the regularization parameter  $\alpha$  must be carefully selected in the traditional Tikhonov regularization.

Suppose that  $\tau=1.4$ . The iterative Tikhonov regularization is carried out when  $\alpha=10^{-6}$  and  $\alpha=10^{-5}$  respectively. When  $\alpha=10^{-6}$ , the iteration numbers of the inverse calculation at 20 points of time in a period are [1 1 1 1 2 1 1 1 1 2 2 2 1 1 1 1 1 2]. When  $\alpha=10^{-5}$ , the iteration numbers are [4 4 4 4 3 5 5 2 4 4 2 2 4 4 3 5 2 4]. Thus, the iteration number increases when the selected value of  $\alpha$  is unsatisfactory. Figure 5 presents the comparison among the accurate voltages and the inverse solutions of the iterative regularization in a sinusoidal period. Figure 5 shows that the difference between the two inverse solutions is insignificant when  $\alpha$  approaches two different values. Therefore, the iterative Tikhonov regularization method with the variable of the iteration number can decrease the susceptibility of  $\alpha$  to the inverse solution by adjusting the number of iterations.

The iterative Tikhonov regularization is carried out successively based on 20 sets of measured data in a sinusoidal period. The iteration number varies each time, but is certainly no more than 5. The simulation is conducted with a regular computer configuration with Intel Core I5 CPU, 3.2 GHz clock and 4 GB frequency of memory. It takes 0.012s for calculation using MATLAB software. The speed of calculation is acceptable.

The RMS and phase of the three-phase voltages are extracted from the sinusoidal fitting curves on the basis of the 20 sets of real-time inverse solutions in a period. The results of the three-phase voltage phasors are statistically shown in Table 2. Moreover, the root-mean-square errors (RMSEs) between the inverse solutions and the accurate values are computed to reflect the deviation of the inverse solutions from the accurate values.

Table 2 also shows that the point-by-point iterative Tikhonov regularization is superior to other methods in terms of accuracy.

The point-by-point iterative Tikhonov regularization with  $\alpha = 10^{-6}$  is adopted under different measurement error levels. Tables 3 and 4 show the results.

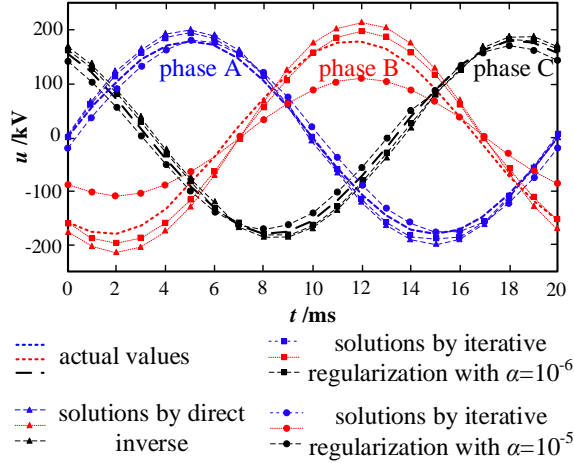


Fig. 4. Comparison among actual values, directly inverse solutions, and single regularization solutions.

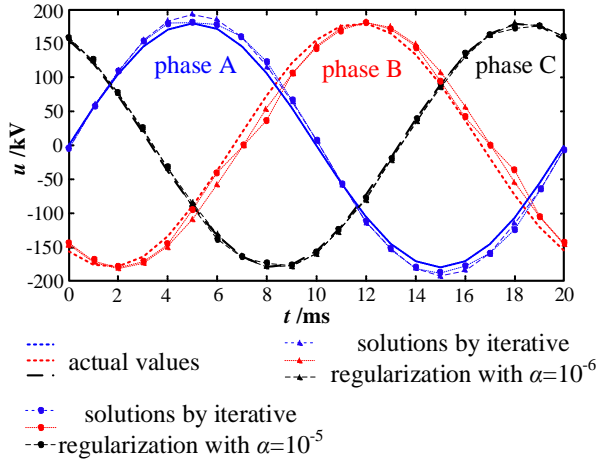


Fig. 5. Comparison among actual values and iterative regularization solutions.

Various factors affect measurements in a real complicated engineering environment; thus, a measurement error of up to 25% is set in the example. Tables 3 and 4 show that the error of solution increases as the measurement error increases. However, when the measurement error is less than 20% in Case I and less than 15% in Case II, the accuracy of the inverse solutions calculated on the basis of the proposed position optimization and point-by-point iterative Tikhonov regularization is satisfactory. For many other methods, the inverse solutions almost deviate from the actual values when the measurement error exceeds 10%. The analysis results of the examples verify the accuracy and robustness of the presented method.

#### IV. EXPERIMENTAL VERIFICATION

Figure 6 presents the simulation experimental platform of the three-phase AC OTLs. The real-time electric field data are synchronously measured by the

three self-made devices.

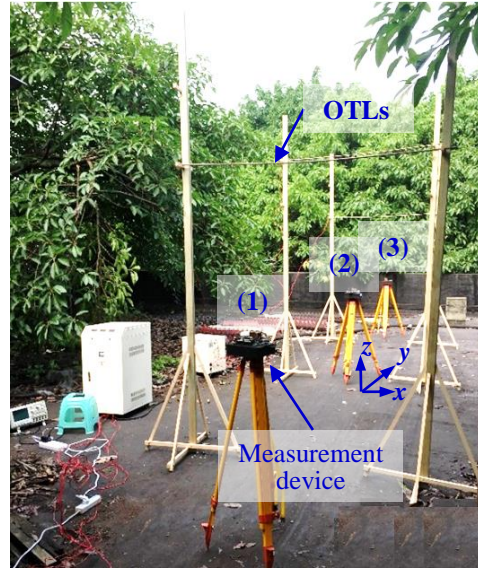


Fig. 6. Experimental site.

The three-phase AC voltages on OTLs are measured by a system that contains high-voltage probes and oscilloscope. They do not show complete three-phase symmetry:

$$\dot{U} = \begin{bmatrix} \dot{U}_A \\ \dot{U}_B \\ \dot{U}_C \end{bmatrix} = \begin{bmatrix} 9.26 \angle -158^\circ \\ 8.91 \angle -33^\circ \\ 8.47 \angle 83^\circ \end{bmatrix} \text{ kV} \cdot$$

Figure 7 shows the measured  $E_z$  components at three points.

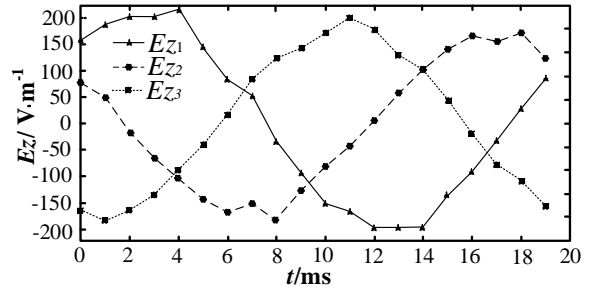


Fig. 7. Measured  $E_z$  at three points in the time-domain.

The iterative Tikhonov regularization with  $\alpha = 10^{-4}$  is adopted to inversely calculate the three-phase voltages point by point in the time domain. The comparison between actual values and the solutions is shown in Fig. 8. The phasors of the three-phase voltage can be obtained by sine curve fitting:

$$\dot{U}^\delta = \begin{bmatrix} \dot{U}_A^\delta \\ \dot{U}_B^\delta \\ \dot{U}_C^\delta \end{bmatrix} = \begin{bmatrix} 9.25 \angle -154^\circ \\ 8.89 \angle -30^\circ \\ 8.51 \angle 88^\circ \end{bmatrix} \text{ kV} \cdot$$

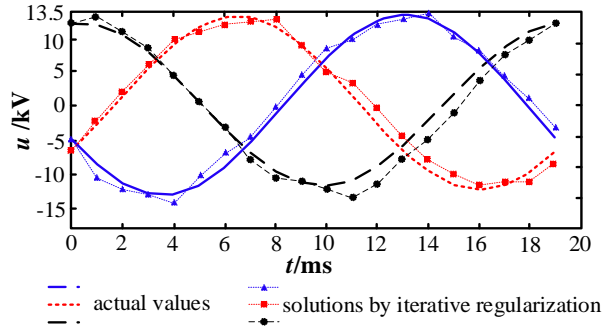


Fig. 8. Comparison between actual values and solutions of three-phase voltages.

The maximum RMS error and phase error of the calculated three-phase voltages are 10 V and 5°, respectively. This result shows that the proposed non-contact measurement of voltage on OTLs has engineering feasibility and accuracy

### V. CONCLUSION

The aim of the study is to realize the non-contact measurement of voltages on AC OTLs through inverse calculation based on measured electric field data under OTLs. An accurate mathematical model and modified inverse solution algorithms are proposed to improve the accuracy, stability, and robustness of the inverse calculation. They are summed up as follows.

An accurate 3-D mathematical model between the voltages and the electric fields of OTLs is built with

consideration of the real engineering environment and physical form of OTLs.

The position optimization of measuring points is presented to minimize the condition number of the observation matrix and reduce the sensitivity of inverse solutions to measurement noise. The particle swarm algorithm for position optimization is proved to perform well in global optimization.

The iterative Tikhonov regularization method with varying iteration numbers is developed to further improve the ill-posedness of inverse problems. Compared with the traditional Tikhonov regularization method, the method presented avoids the complex computation of selecting regularization parameters  $\alpha$  and decreases the susceptibility of  $\alpha$  to inverse solutions by adjusting the number of iterative calculations.

The process of point-by-point regularization performs real-time correction for the inverse calculation, thereby improving the calculation accuracy.

The analysis results of the given examples and experiments verify that through the combination of the above four improvements, inverse solutions with satisfactory accuracy can be obtained under the condition with high measurement errors. Moreover, the rapidity, stability, and robustness of the inverse calculation are demonstrated.

### ACKNOWLEDGMENT

This work was supported by the National Natural Science Foundation of China (NSFC 51407016, 51577017) and National "111" Project of China (Grant No. B08036).

Table 1: Comparison of the inverse solutions when setting different measuring points

Measuring Positions ( $x_k y_k z_k$ )/m	Cond( $\mathbf{K}$ )	Inverse Solution $\mathbf{U}^{\delta}$	
		Mean Value/kV	Variance (RMS Phase)
$\begin{cases} (10 & -5 & 1) \\ (10 & 0 & 1) \\ (10 & 5 & 1) \end{cases}$	266.44	A: $[139.92 \angle -1.72^\circ]$	(47.02 23.54)
		B: $[216.10 \angle -58.57^\circ]$	(162.10 105.55)
		C: $[135.13 \angle 121.37^\circ]$	(49.13 26.59)
$\begin{cases} (100 & -10 & 2) \\ (100 & 0 & 2) \\ (100 & 10 & 2) \end{cases}$	36.66	A: $[141.36 \angle 1.59^\circ]$	(18.73 2.84)
		B: $[166.62 \angle -125.94^\circ]$	(32.19 18.79)
		C: $[129.41 \angle 118.32^\circ]$	(10.03 7.33)
$\begin{cases} (150 & -7.5 & 3) \\ (150 & 0 & 3) \\ (150 & 7.5 & 3) \end{cases}$	14.87	A: $[128.74 \angle -0.967^\circ]$	(13.37 1.67)
		B: $[121.33 \angle -121.51^\circ]$	(22.31 11.21)
		C: $[124.35 \angle 121.22^\circ]$	( 8.19 3.81)

Table 2: Statistics of various inverse solutions of three-phase voltages

Accurate Values	Directly Inversion	Single Regularization when $\alpha=10^{-6}$	Single Regularization when $\alpha=10^{-5}$	Iterative Regularization when $\alpha=10^{-6}$	Iterative Regularization when $\alpha=10^{-5}$
127.02∠0°	140.48∠1.01°	138.17∠-0.17°	127.07∠-6.55°	132.22∠-1.22°	131.37∠-1.28°
127.02∠-120°	151.84∠-126.40°	139.30∠-126.45°	77.22∠-126.80°	128.55∠-124.45°	127.91∠-126.90°
127.02∠120°	131.64∠115.78°	129.82∠117.17°	121.41∠124.56°	128.27∠118.37°	129.41∠118.83°
RMSE of RMS	16.54	9.73	28.92	3.21	2.92
RMSE of Phase	4.46	4.07	6.05	2.83	4.11

Table 3: Statistics of inverse solutions obtained under different measurement errors in Case I

Measurement Error/ %	$\dot{U}_A^\delta/\text{kV}$	$\dot{U}_B^\delta/\text{kV}$	$\dot{U}_C^\delta/\text{kV}$	RMSE of RMS	RMSE of Phase
0	127.02∠0°	127.02∠-120°	127.02∠120°	0	0
± 5	128.85∠0.29°	129.26∠-120.23°	128.35∠119.83°	1.86	0.24
± 10	132.22∠-1.22°	128.55∠-124.45°	128.27∠118.37°	3.21	2.83
± 15	123.40∠-1.24°	134.77∠-122.44°	130.67∠113.45°	5.38	4.09
± 20	115.22∠-2.61°	121.12∠-114.02°	133.07∠112.85°	8.37	5.58
± 25	133.94∠3.07°	140.24∠-112.87°	137.68∠137.91°	10.61	11.27

Table 4: Statistics of inverse solutions obtained under different measurement errors in Case II

Measurement Error/ %	$\dot{U}_A^\delta/\text{kV}$	$\dot{U}_B^\delta/\text{kV}$	$\dot{U}_C^\delta/\text{kV}$	RMSE of RMS	RMSE of Phase
0	127.02∠0°	127.02∠-120°	127.02∠120°	0	0
± 5	124.21∠0.79°	130.25∠-115.25°	131.24∠119.06°	3.48	2.88
± 10	121.77∠0.75°	131.15∠-113.16°	134.06∠117.74°	5.61	4.18
± 15	131.25∠-1.15°	139.78∠-124.06°	121.83∠113.87°	8.33	4.29
± 20	125.28∠-2.27°	108.45∠-112.70°	130.36∠128.11°	10.93	6.43
± 25	137.11∠4.37°	151.43∠-115.96°	138.09∠108.25°	16.55	7.60

## REFERENCES

- [1] C. Venkatesh and K. S. Swarup, "Performance assessment of distance protection fed by capacitor voltage transformer with electronic ferro-resonance suppression circuit," *Electric Power Systems Research*, vol. 112, pp. 12-19, 2014.
- [2] D. Topolaneck, M. Lehtonen, and M. R. Adzman, "Earth fault location based on evaluation of voltage sag at secondary side of medium voltage/low voltage transformers," *IET Generation Transmission & Distribution*, vol. 9, no. 14, pp. 2069-2077, 2015.
- [3] Z. Tong, Z. Dong, and T. Ashton, "Analysis of electric field influence on buildings under high-voltage transmission lines," *IET Science Measurement & Technology*, vol. 10, no. 4, pp. 253-258, 2016.
- [4] A. M. Farah, M. Afonso, and A. Vasconcelos, "A finite-element approach for electric field computation at the surface of overhead transmission line conductors," *IEEE Magnetics Society*, vol. PP, no. 99, pp. 1-4, 2017.
- [5] R. M. Sarmento, "Electric and magnetic fields in overhead power transmission lines," *IEEE Latin America Transactions*, vol. 10, no. 4, pp. 1909-1915, 2012.
- [6] R. M. Radwan, A. M. Mahdy, and M. Abdel, "Electric field mitigation under extra high voltage power lines," *IEEE Trans. Dielectrics and Electrical Insulation*, vol. 20, no. 1, pp. 54-62, 2013.
- [7] F. Yang, H. Wu, and W. He, "Investigation on the electric field inverse problem of HV transmission lines and discussion on its application," *ACES Journal*, vol. 25, no. 2, pp. 129-136, 2010.
- [8] A. Z. E. Dein, "Parameters affecting the charge distribution along overhead transmission lines"

- conductors and their resulting electric field,” *Electric Power Systems Research*, vol. 108, pp. 198-210, 2014.
- [9] A. Ilyin, S. I. Kabanikhin, and D. B. Nurseitov, “Analysis of ill-posedness and numerical methods of solving a nonlinear inverse problem in pharmacokinetics for the two-compartmental model with extravascular drug administration,” *Journal of Inverse and Ill-Posed Problems*, vol. 20, pp. 39-64, 2012.
- [10] S. Lu and J. Flemming, “Convergence rate analysis of Tikhonov regularization for nonlinear ill-posed problems with noisy operators,” *Inverse Problems*, vol. 28, pp. 104003, 2012.
- [11] T. Ogawa, “Complex-valued network inversion with regularization for ill-posed inverse problems,” *Computer Technology & Application*, vol. 3, pp. 408-417, 2012.
- [12] Z. Zhang, Z. Zhu, and Q. Xin, “Analysis and application of inverse detecting method based on local electric field,” *ACES Journal*, vol. 27, no. 7, pp. 566-573, 2012.
- [13] S. I. Kabanikhin, *Inverse and Ill-posed Problems*. DE GRUYTER, Berlin, 2011.
- [14] J. Xu, F. Schreier, and A. Doicu, “Assessment of Tikhonov-type regularization methods for solving atmospheric inverse problems,” *Journal of Quantitative Spectroscopy and Radiative Transfer*, vol. 184, pp. 274-286, 2016.
- [15] H. Mao, “Adaptive choice of the regularization parameter in numerical differentiation,” *Journal of Computational Mathematics*, vol. 33, pp. 415-427, 2015.
- [16] C. Shi, C. Wang, and G. Zheng, “A new posteriori parameter choice strategy for the convolution regularization of the space-fractional backward diffusion problem,” *Journal of Computational and Applied Mathematics*, vol. 279, pp. 233-248, 2015.
- [17] J. L. García Pallero, J. L. Fernández-Martínez, and Z. Fernández-Muñiz, *The Effect of the Noise and the Regularization in Inverse Problems: Geophysical Implication*, Mathematics of Planet Earth, Springer, Berlin Heidelberg, 2014.
- [18] P. Kumar and A. K. Singh, *Single Measurement Based Mechanical State Estimation for Overhead Transmission Lines with Level Spans*. IEEE Press, New Jersey, 2014.
- [19] F. Bassi, G. Giannuzzi, and M. Giuntoli, “Mechanical behaviour of multi-span overhead transmission lines under dynamic thermal stress of conductors due to power flow and weather conditions,” *International Review on Modelling & Simulations*, vol. 6, pp. 1112-1122, 2013.
- [20] F. Liu and R. D. Findlay, “Investigation of mechanical properties of single layer ACSR based on an integrated model,” *Electric Power Systems Research*, vol. 78, pp. 209-216, 2008.
- [21] P. G. Huray, *Static Electric Fields Maxwell's Equations*. Wiley-IEEE Press, USA, 2010.
- [22] S. S. Chowdhury, A. Lahiri, and S. Chakravorti, “Surface resistance modified electric field computation in asymmetric configuration using surface charge simulation method: a new approach,” *IEEE Trans. Dielectrics & Electrical Insulation*, vol. 19, no. 3, pp. 1068-1075, 2012.
- [23] R. Djekidel, C. Abdelghani, and H. Abdechafik, “Efficiency of some optimization approaches with the charge simulation method (CSM) for calculating the electric field under EHV power lines,” *IET Generation Transmission & Distribution*, vol. 11, no. 17, pp. 4167-4174, 2017.
- [24] D. Xiao, Y. Xie, and H. Liu, “Position optimization of measuring points in voltage non-contact measurement of AC overhead transmission lines,” *ACES Journal*, vol. 32, no. 10, pp. 908-914, 2017.
- [25] F. Chen and Y. B. Tian, “Modeling resonant frequency of rectangular microstrip antenna using CUDA-based artificial neural network trained by particle swarm optimization algorithm,” *ACES Journal*, vol. 29, no. 12, pp. 1025-1034, 2014.
- [26] M. Grasmair, “Variational inequalities and improved convergence rates for Tikhonov regularisation on banach spaces,” *Journal of Inverse and Ill-Posed Problems*, vol. 21, pp. 379-394, 2013.
- [27] S. George and M. Kunhanandan, “An iterative regularization method for ill-posed Hammerstein type operator equation,” *Journal of Inverse and Ill-posed Problems*, vol. 17, pp. 831-844, 2009.



**Dongping Xiao** received the B.Sc. degree in Industrial Automation from Chongqing University, Chongqing, China, in 1999, and the M.Sc. and Ph.D. degrees in Electrical Engineering from Chongqing University, in 2004 and 2009, respectively. From 2012 to 2013, she was a Visiting Scholar with Washington State University, USA. Currently, she is an Associate Professor at the College of Electrical Engineering, Chongqing University, China. Her main fields of interests include calculation and simulation of electromagnetic field, electromagnetic measurement and running state monitoring of power transmission equipment.